scientific reports

OPEN

Enhancement of electroless copper coatings by triazole dithiocarbamate and green additives

Palanivelu Balaramesh[1,7]✉, Raja Venkatesan[2,3]✉, Suseela Jayalakshmi[4], Shanmugam Kotteswaran[4], Eswaran Kamaraj[5,7], Alexandre A. Vetcher[6] & Seong-Cheol Kim[3]✉

This work explores the deposition of nanoscale copper utilizing five different electroless bath formulations based on xylitol. Good complexation, reduction, and pH control were demonstrated in the first bath using xylitol, glyoxylic acid, and potassium hydroxide. A modified version included 1,2,4-triazole (Tz), which served as a stabilizing agent and a strong inhibitor. To enhance environmental compatibility and regulate deposition behavior, later formulations included chitosan (CS), triazole dithiocarbamate (TzDTC), and methanesulfonic acid (MSA) at a concentration of one part per million. Copper deposition was effectively accomplished at pH 12.75 and 45 °C. The optimized additive combination improved corrosion resistance, as evidenced by a drop in icorr from 58.3 to 41.8 mA/cm^2, reduced surface roughness from 155.8 nm (plain bath) to 19.0 nm (brightener bath), and reduced the amount of deposit from 3.46 per hour to 2.68 µm/h. The specific surface area increased in conjunction with the crystallite size falling from 24.07 to 20.17 nm. TzDTC significantly changed the electrochemical and physical characteristics of the bath. In contrast, CS improved the smoothness and homogeneity of the copper layer that was deposited by acting as a brightener and leveling agent. The article describes the resulting shiny copper coatings and methodically assesses the additives' inhibitory and accelerating effects. Surface texture was assessed using XRD and atomic force microscopy (AFM), and corrosion behavior was evaluated using cyclic voltammetry and Tafel polarization.

Keywords Xylitol, Glyoxylic acid, Brightener, Chitosan, Eco-friendly

Electroless plating is widely used to apply consistent, superior metal finishes to complicated or non-metallic surfaces because it has a number of benefits over conventional electroplating techniques. This method may cover items with intricate geometries because it guarantees uniform coating thicknesses and robust binding between the coated metal layer and the underlying substrate. It is utilized in many sectors, such as electronics, transportation, aviation, and jewellery, and is beneficial for metals like copper, nickel, gold, and silver[1–4]. For example, electroless copper plating is widely used because of its higher wear resistance, corrosion resistance, and durability. While electroplating depends on an external electrical current to move metal ions to a surface, electroless plating is a chemical process powered by a redox reaction.

This technique uses no electricity to decrease and deposit metal ions onto a substrate. This special quality makes electroless plating a flexible and effective way to make metal coatings[5–8]. In electroless copper plating, xylitol, a natural sugar alcohol, is a common complexing agent due to its potent stabilizing properties. Xylitol is a green, biodegradable substance with several advantages over traditional complexing agents, many of which are

[1]Department of Chemistry, R.M.K. Engineering College, Chennai, Tamil Nadu 601206, India. [2]Department of Biomaterials, Saveetha Dental College and Hospitals, SIMATS, Saveetha University, Chennai, Tamil Nadu 600077, India. [3]School of Chemical Engineering, Yeungnam University, 280 Daehak-ro, Gyeongsan 38541, Republic of Korea. [4]Department of Chemistry, Vels Institute of Science, Technology and Advanced Studies, Chennai, Tamil Nadu 600117, India. [5]Department of Chemistry, Yeungnam University, 280 Daehak-ro, Gyeongsan 38541, Republic of Korea. [6]Institute of Pharmacy and Biotechnology (IPhB), RUDN University n.a. P. Lumumba (RUDN), 6 Miklukho-Maklaya Str, Moscow 117198, Russian Federation. [7]Palanivelu Balaramesh and Eswaran Kamaraj have contributed equally to this work. ✉email: pbr.sh@rmkec.ac.in; rajavenki101@gmail.com; sckim07@ynu.ac.kr

made from hazardous or toxic ingredients. Its environmental friendliness makes it a desirable choice for creating more sustainable and ecologically conscious plating procedures.

Conventional electroless copper baths frequently have poor corrosion resistance, limited adhesion, coarse-grain development, and instability. The creation of better formulations with additives that increase coating uniformity, crystallinity, and long-term durability is motivated by these shortcomings. Furthermore, there has been a significant movement toward greener, biodegradable substitutes due to the safety and environmental concerns around conventional complexing and reducing agents. Xylitol, glyoxylic acid, and other bio-derived modifiers offer a sustainable solution to control deposition kinetics, stabilize bath chemistry, and produce high-quality copper coatings with less of an adverse effect on the environment[9–12].

Another interesting reduction agent in electroless copper coating is glyoxylic acid, a small organic molecule. Glyoxylic acid, which is renowned for its effectiveness and environmental friendliness, is necessary for the transformation of copper ions (Cu^{2+}) into their metallic form (Cu), which promotes copper deposition. It is a helpful agent in the plating bath because of its special structure, which includes both an aldehyde and a carboxyl group. This structure effectively transfers electrons and decreases copper ions[13–17].

Electroless copper plating baths benefit from the addition of methanesulfonic acid (MSA). In addition to raising the overall plating rate for more effective deposition, MSA stabilizes the copper bath, improving the regularity and uniformity of copper deposits. Because MSA is safer, less hazardous, and more biodegradable than conventional acids, it is a superior choice for businesses looking to implement more environmentally conscious practices. It also makes copper layers smoother and stickier, making them suitable for high-precision sectors like circuit design and electronics[18–23].

In electroless copper plating, the heterocyclic molecule 1,2,4-triazole is utilized as a stabilizer. By releasing copper ions for regulated reduction, it makes the copper plating solution more stable. Furthermore, 1, 2, 4-triazole slows down the rate of deposition to avoid an excessive or uneven copper accumulation[24,25]. To improve the electroless copper plating process, triazole dithiocarbamate is another essential ingredient. It improves the physical and electrochemical characteristics of the copper deposits by stabilizing and changing them[26]. It is perfect for high-performance applications like electronics and microelectronics because it produces smoother, more uniform coatings with exact thickness and greater adhesion by controlling the deposition rate[27]. The longevity and endurance of the copper deposits are increased by their resistance to corrosion, even in challenging conditions[28].

An integral part of electroless copper plating is chitosan, a non-toxic, biodegradable substance made from renewable resources. The increasing need for sustainable production methods aligns with its eco-friendly attributes. By serving as a leveller and brightener, chitosan enhances the glossy look and smoothness of copper coatings[29–32]. The combined and sequential effects of xylitol, MSA, triazole derivatives, and chitosan on bath stability, autocatalytic reduction kinetics, crystal growth orientation, and corrosion resistance have not yet been thoroughly studied in electroless copper systems. The combined effects of these additives on nucleation, inhibition/acceleration balance, and microstructural development have not been assessed in systematic research.

This study aims to systematically investigate how sequentially introduced green additives—triazole (Tz), methanesulfonic acid (MSA), triazole dithiocarbamate (TzDTC), and chitosan (CS)—modulate the autocatalytic copper-reduction behaviour of a xylitol-based electroless bath. Specifically, the work evaluates how the successive incorporation of these additives influences the structural, morphological, and electrochemical characteristics of the resulting electroless copper coatings.

Materials and methods

Materials

All chemicals obtained from Sigma-Aldrich, Fisher, Merck, and S.D. Chemicals, India, were of the highest analytical grade (≥ 99% purity) and used as received without further purification. The materials employed included xylitol ($C_5H_{12}O_5$), glyoxylic acid ($C_2H_2O_3$), methanesulfonic acid (CH_4O_3S), 1,2,4-triazole ($C_2H_3N_3$), triazole dithiocarbamate anion ($C_4H_4N_4S_2^-$), chitosan ($(C_6H_{11}NO_4)_n$), potassium hydroxide (KOH), copper carbonate ($CuCO_3$), $KMnO_4/H_2SO_4$ cleaning solutions, and $SnCl_2/PdCl_2$ sensitization–activation solutions. All the stock solutions were made with water that has been double-distilled.

Experimental

Environmentally friendly electroless copper electrolytes were prepared using analytical-grade reagents, including potassium hydroxide, xylitol, glyoxylic acid, triazole (Tz), methanesulfonic acid (MSA), triazole dithiocarbamate (TzDTC), and chitosan (CS). Electroless deposition was carried out on BIS-F epoxy substrates (FR-4 grade, 1.6 mm thickness) placed in a 100-cc beaker.

The substrates were first mechanically polished using successive alumina grit papers (400–1200 mesh) and then rinsed thoroughly with double-distilled water. Chemical cleaning was performed using a $KMnO_4$ (0.1 M) and H_2SO_4 (1 M) solution for 5 min at 50 °C, followed by rinsing with distilled water. Immersion into a 0.05 M $SnCl_2$ mixture containing 0.1 M HCl for three minutes resulted in sensitization.

The substrates were then treated with 0.001 M $PdCl_2$ in 0.1 M HCl for two minutes to create the active catalytic surface. Electroless copper deposition was then carried out after the samples had been thoroughly cleaned with distilled water. The repeatability of the plating process and uniform surface activation are guaranteed by this thorough technique. The compositions of the electroless copper baths used in this study are summarized in Table 1.

Calculating the deposit rate

The following formula was applied to determine the rate of copper deposits:

S. No	Bath Components	Plain xylitol bath (PB)	Chemical ingredients with xylitol PB			
1	Cu^{2+} concentration (g/L)	3	3	3	3	3
2	Xylitol (g/L)	20	20	20	20	20
3	Glyoxylic acid (g/L)	10	10	10	10	10
4	pH (KOH)	12.75	12.75	12.75	12.75	12.75
5	Temperature (°C)	45	45	45	45	45
6	Tz, (ppm)	–	1	1	1	1
7	MSA (ppm)	–	–	1	1	1
8	TzDTC (ppm)	–	–	–	1	1
9	CS (ppm)	–	–	–	–	1

Table 1. The chemical constitution of a plain bath optimized with xylitol and additives. Every measurement was carried out at least three times.

$$Rate\,of\;deposition\;(\mu m/h)\;T\;=\;W\;\times\;10^{-4}/dAt \tag{1}$$

where “W” stands for the deposit’s weight (g), “d” for copper’s density (8.96 g/cm^3), “A” for the plated sheet’s square area in centimeters, and “t” for the protection period in hours.

The following basic relationship has been used to determine the electroless copper coating quantity:

$$The\,rate\,of\;deposition\;(\mu m/h)\;=\;Thickness\;/\;Deposition\,rate \tag{2}$$

Calculating the copper deposit’s thickness

A formula as follows has been employed to determine the thickness of the copper deposits:

$$Thickness\;(\mu m)\;=\;W\;\times\;10^{-4}\;\times\;60\;/\;A\;\times\;D \tag{3}$$

The deposition time is converted from minutes to hours in Eq. 3 by the factor 60. “W” stands for the weight of the deposited copper (g), “A” for the plated area (cm^2), and “D” for the copper density (8.96 g/cm^3). By deducting the original weight of the sample from its weight following plating, the deposit weight (W) is calculated. This method guarantees precise computation of the thickness of the copper layer under the designated experimental conditions.

where: W = (w_1 – w_2) is the deposit’s weight (g), After plating, weight (g) = w_1, After stripping, weight (g) = w_2, “A” stands for the substrate’s entire plated area, expressed in centimetres squared, “D” represents the density of copper.

Characterization

Atomic force microscope (AFM)

A Swiss Nano Surf Easy Scan2 (AFM) has been employed to analyze the copper deposits’ roughness on the surface. This approach differs from previous electron microscopes in that it can obtain an accuracy of 10 pm and evaluate materials in both solutions and gases.

X-ray diffraction (XRD)

The structural features of the copper deposits were determined using the technique of X-ray diffraction (X'Pert-Pro, P-Analytical). The Debye–Scherrer equation was employed to estimate the average crystallite size, rather than particle size, based on diffraction peak broadening.

$$D\;=\;K\lambda\;/\;\beta cos\theta \tag{4}$$

Here, K represents the Scherer constant, λ denotes the wavelength of the diffraction light, β serves as the Full Width at Half Maximum (FWHM) of the sharp peaks, and θ indicates the diffraction angle[33,34].

The Scherrer factor (K) is frequently set as 0.89 to account for the size and form of the crystallites. The formula below is used to determine the specific surface area of the copper deposit.

In this case, "d" stands for the anticipated density of the copper (8.96 g/cm2) and "D" for the crystallite structures’ dimensions (in nm).

The ratio SSA = 6/ (D × ρ) was used to determine the specific surface area (SSA), assuming spherical crystallites.

where: ‘D’ is the crystallite size (nm), ‘ρ’ is the density of copper (8.96 g/cm^3).

The following formula yields the crystallinity fraction, “Xc”

$$XC\;=\;\{0.24\;/\;\beta\}^3 \tag{5}$$

Microstrain (ε) was calculated using the conventional Williamson–Hall Uniform Deformation Model (UDM), which relates peak broadening to strain as

$$\varepsilon = \beta / (4 \tan\theta) . \tag{6}$$

Dislocation density is calculated as:

$$(\delta) = 1 / D^2 \tag{7}$$

The unit cell volume "V" is obtained by $V = a^3$, using the lattice constant for the copper FCC structure (JCPDS card no. 04-0836), where a = 0.361491 nm[35].

Cyclic voltammetry (CV)
A traditional electrochemical detector was used to perform cyclic voltammetric studies. To eliminate dissolved oxygen, nitrogen dioxide was used to purge the copper methanesulfonate solution before analysis. The reference electrode was an Ag/AgCl electrode treated with KCl, and the counter electrode was a platinum wire. The Ag/AgCl (3 M KCl) reference electrode is used to report all potentials obtained throughout the cyclic voltammetry measurements. The working electrode was a polished glassy carbon conducting material, and the supporting electrolyte was 0.1 M Na_2SO_4. The voltametric study was conducted at room temperature (27 °C). The voltage graphs were captured at a scan rate of 50 mV s^{-1} spanning the potential range of −1.2 to + 0.5 V.

The selected scan rate of 50 mV s^{-1} provided rapid qualitative insight into the reduction behavior and film-formation tendencies of the system. It was acknowledged that this relatively high scan rate introduces diffusion-controlled contributions and prevents the establishment of steady-state conditions; therefore, the cyclic voltammetry results are interpreted only for comparative trends rather than for quantitative mechanistic evaluation of corrosion kinetics. To confirm correct normalization about electrode surface area, all electrochemical graph is provided in terms of current density (mA cm^{-2}) rather than absolute current.

Tafel polarization
Polarization curves for anodic and cathodic processes were obtained by applying potentials sufficiently displaced from the corrosion potential and recording the corresponding current response. The linear parts of the log I versus potential graphs were used to identify the Tafel areas. The anodic and cathodic Tafel curves were extended to their junction at the potential for corrosion (Ecorr) to estimate the density of corrosion currents (icorr).

The copper reduction current was derived directly from the cathodic Tafel slope (βc), independent of the glyoxylic acid oxidation contribution, following the Stern–Geary equation. The corrosion rate was calculated using icorr together with Faraday's law. This approach is based on the classical Stern–Geary framework for quantitative corrosion analysis. Tafel observations were performed at a scan rate of 0.5 mV s^{-1}, which is within the suggested range of 0.1–1 mV s^{-1} to guarantee accurate icorr and ecorr measurement without distortion from diffusion or capacitive effects[36]. To guarantee uniformity across all electrochemical tests, the Ag/AgCl (3 M KCl) electrode is used as a reference for all potential values derived from the polarization experiments.

$$icorr = (\beta a \times \beta c) / [2.303 \times (\beta a + \beta c) \times Rp] \tag{8}$$

where; "Rp" stands for polarization resistance.

Results and discussion

There were five distinct electroless copper baths made with xylitol that were connected. As shown in Table 1, the component complexes along with the reducing agent in the initially created bath compositions are xylitol with glyoxylic acid, respectively. At 45 °C, the pH had been adjusted to 12.75 utilizing KOH adjustment. The first electroless copper bath is called the xylitol plain bath (PB) because the four additions that follow change the copper deposits' varied qualities.

The second, third, fourth, and fifth formulations are referred to as the stabilizer, eco-friendly, modifier, and brightener baths, respectively. The term 'brightener bath' denotes formulations containing additives that promote smoother, more reflective surfaces; such brightness is typically associated with finer grain structures and reduced surface roughness. Physical characteristics, such as coating thickness and deposition rate, were assessed; Table 2 demonstrates that these values gradually decrease with the addition of stabilizers and additives. As a result, these additives function as efficient inhibitors, controlling the kinetics of deposition and enhancing the electroless copper coatings' quality.

				Structural Properties		
		Physical properties		XRD		AFM
S. No	Bath components / (Bath code)	Rate of deposition (µm/h)	Thickness (µm)	Size of crystallites (nm)	Specific area of surface (m^2/g)	Roughness (nm)
1	Simple xylitol bath (PB) / (B1)	3.46	207.6	24.07	27.820	155.849
2	Xylitol PB + Tz / (B2)	3.09	185.4	22.22	30.136	112.688
3	Xylitol PB + Tz + MSA / (B3)	3.02	181.2	20.55	32.586	48.597
4	Xylitol PB + Tz + MSA + TzDTC / (B4)	2.76	165.6	20.47	32.713	38.447
5	Xylitol PB + Tz + MSA + TzDTC + CS / (B5)	2.68	160.8	20.17	33.199	18.997

Table 2. Physical and structural properties of the electroless deposition baths B1, B2, B3, B4, and B5.

The most used metric for measuring surface roughness is average roughness (Ra), and AFM offers high-resolution topographical analysis to get these values. Smoother surfaces and higher-quality metal films are often indicated by lower Ra values. Ra values in the wide range of 5–500 nm may be found in electroless copper coatings; however, films with Ra < 100 nm are usually regarded as preferable because of better adhesion, lower scattering losses, and smoother microstructural characteristics.

The consecutive addition of additives significantly affects surface roughness in all plating baths, as Table 2 and Fig. 1 illustrates. Ra in the plain xylitol bath started at 155.849 nm and gradually dropped with each addition. With the lowest roughness (Ra = 18.997 nm), the brightener-modified bath demonstrated significant surface leveling. This methodical decrease in Ra indicates that the additives successfully encourage more uniform coating, smoother copper deposition, and improved overall film quality.

By detecting the distinctive diffraction peaks, determining the intended crystallographic orientation without the production of secondary phases, and proving the existence of pure Cu phases, XRD analysis verified the integrity of the electroless copper coatings. To make it easier to identify the crystallographic planes and enhance the interpretability of the structural analysis, the Miller indices (hkl) corresponding to all main diffraction peaks have been added to the XRD patterns (Fig. 2).

The lattice properties and crystalline alignment of the copper deposits were evaluated using X-ray diffraction, with particular attention paid to the primary reflection planes (111), (200), and (220). In copper films generated at lower ion concentrations, the (111) plane usually becomes the dominant orientation since it is known to have the lowest energy at the surface among them. On the other hand, films created with altered bath chemistries or greater ion concentrations may show improved development along higher-energy planes, like (200), which would be indicative of altered surface energetics and deposition kinetics. The observed diffraction fingerprints are generally consistent with a face-centered cubic (FCC) geometry, where the (111) plane represents the most densely packed crystallographic arrangement[23].

Along the (111) plane, the first two plating baths (simple and stabilizer) in Fig. 2 showed a strong reflection. On the other hand, a distinct change toward preferred development along the (200) plane was evident in the remaining three baths. Methanesulfonic acid (MSA), starting with the third bath, is introduced at the same time as this transition. $Cu2+$ availability and solution conductivity are both improved by copper methanesulfonate, which is known to encourage (200)-oriented growth.

More importantly, the shift in preferred orientation is caused by the preferential binding of methanesulfonate anions into the low-energy (111) region. This adsorption increases the effective surface energy of the (111) plane and raises the nucleation overpotential, thereby suppressing (111) growth. Consequently, deposition along the higher-energy (200) plane becomes thermodynamically and kinetically favorable. This mechanistic interpretation aligns with previous reports describing additive-induced orientation switching in electroless

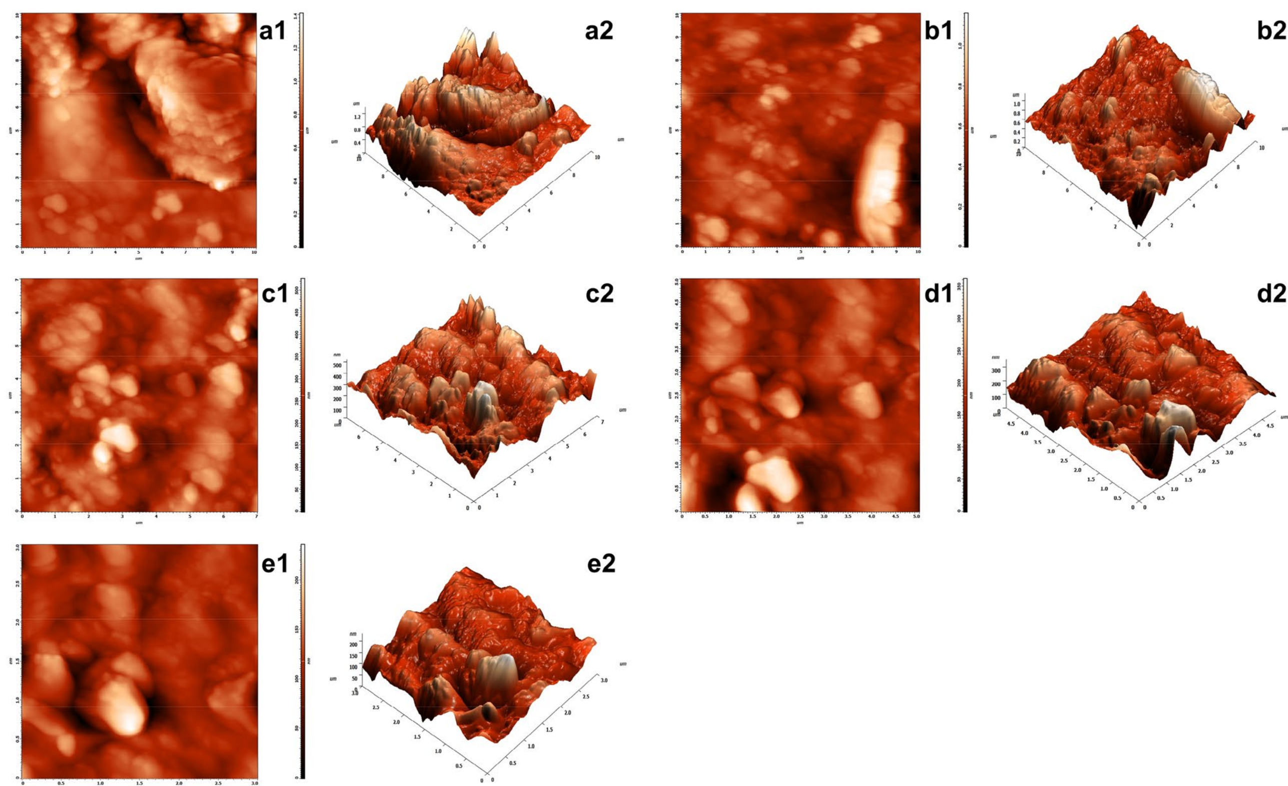

Fig. 1. AFM images of xylitol-based electroless copper baths: (1) surface topography and (2) 3-D morphology of copper deposits for baths (**a**) B1, (**b**) B2, (**c**) B3, (**d**) B4, and (**e**) B5.

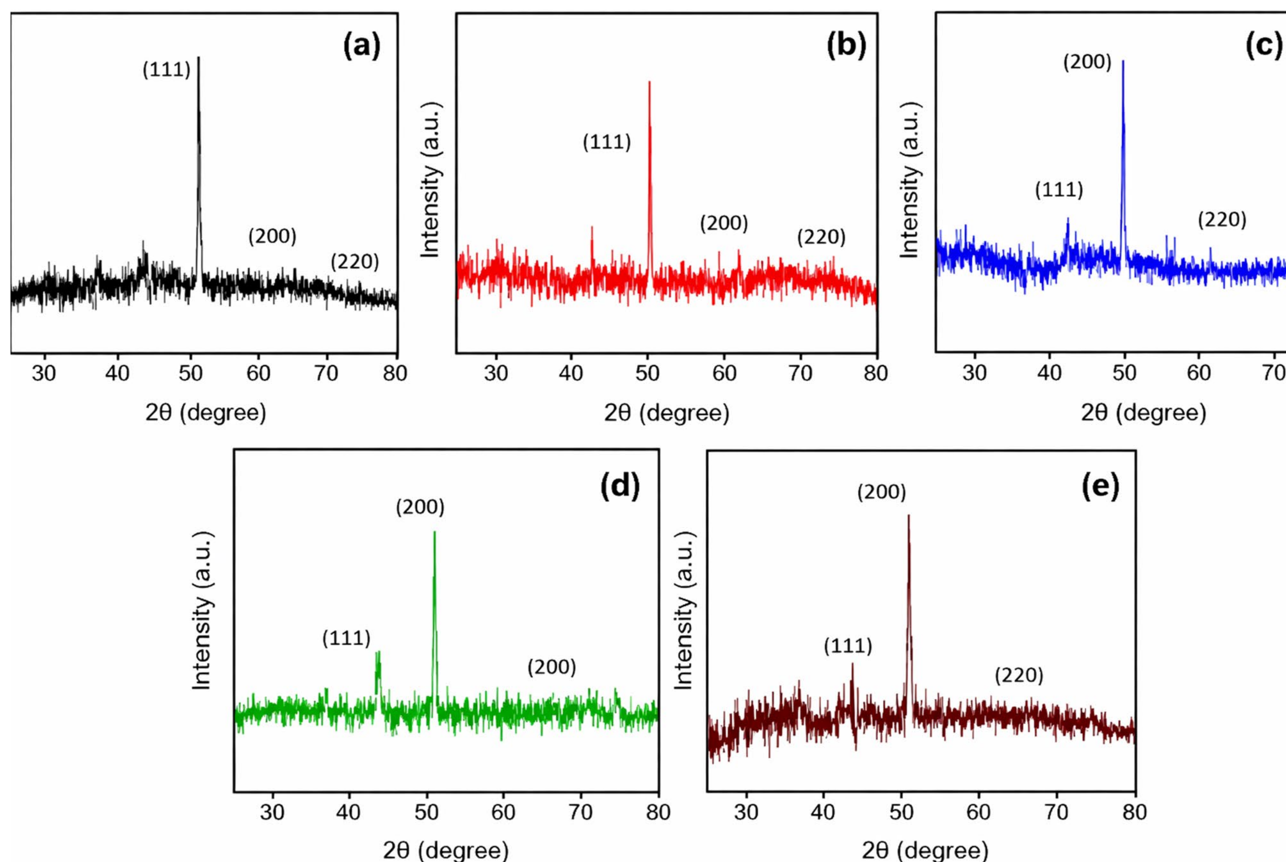

Fig. 2. XRD patterns of electroless copper coatings obtained from xylitol-based baths (**a**) B1, (**b**) B2, (**c**) B3, (**d**) B4, and (**e**) B5.

copper systems. Table 2 shows an inverse correlation between the dimension of the crystallite and the specific area of surface quantity, which is correlated to the line width (FWHM).

When determining dislocation density, the full width and half maximum (FWHM) from XRD information is a critical component. To calculate the crystallinity fraction of the copper deposits, the line width value has been utilized. The dislocation density and the proportion of crystallinity are both strongly influenced by crystallite size. With a cubic closed-packed symmetry, the FCC structure's lattice constant a ' and 'd'-spacing are related to determine the lattice parameters.

The FCC structure's lattice parameters for pure copper are a = b = c = 0.361491 nm, which translates to an approved unit volume of cell (V) of 47.238 nm^3. According to standard FCC copper (JCPDS 04-0836), the distinctive reflections in the XRD patterns at around 43.3°, 50.4°, and 74.1° were indexed as the (111), (200), and (220) planes of reflection, respectively. The Miller indices for each bath composition have been included in the caption of Fig. 2. The reference values stated in the JCPDS 04-0836 file and those provided by the American Society for Testing and Materials ("ASTM") standards are in excellent agreement with the experimental diffraction results.

The deposited copper layer may be assessed using two useful quality control techniques: cyclic voltammetry and Tafel curves. CV and Tafel polarization curves are two examples of these electrochemical characteristics that shed light on the durability, functioning, and surface quality of electroless copper coatings. A lower peak in the CV curve denotes a lower concentration of copper ions (Table 3, Fig. 3). In this study, Ipa-1 indicates the matching anodic peak current, and Epa-1 is the anodic peak potential corresponding to the first oxidation peak shown in the cyclic voltammogram.

The cyclic voltammograms are displayed in terms of current density for uniformity across all electrochemical tests. Therefore, rather than absolute currents, Ipa-1 and Ipc-1 correspond to the anodic and cathodic peak current densities. These electrochemical parameters were used to evaluate the oxidation behavior of copper species and the effect of bath additions on the total electrochemical response. A prominent, crisp anodic peak indicates well-defined oxidation processes and high-quality copper films. Additionally, the cathodic peak potential (Epc-1) shifted negatively when additives were added, indicating improved electrochemical activity and faster reduction kinetics during copper deposition.

To ensure uniformity throughout the electrochemical investigations, all potentials displayed in the Tafel polarization curves and cyclic voltammetry are referenced to the Ag/AgCl (3 M KCl) electrode. The corrosion behavior of the copper deposits is evaluated using Tafel polarization curves (Fig. 4). The corrosion potential (Ecorr) reflects the activity level of the copper deposit; more stability is indicated by a higher Ecorr value.

Bath components (Bath code)	Structural properties				Electrochemical properties			
	Unit cell volume (A^3)	Micro-strain ($10^{-3}lin^2m^{-4}$)	Fraction of crystallinity	Dislocation density (ρ in m/m^3)	E_{pc-1} (mV)	$I_{pc-1} \times 10^{-6}$ (mA cm^{-2})	icorr (μA/cm^2)	Rate of deposition (μm/h)
Xylitol plain bath (PB) (B1)	46.42	5.114	536.85	8.0412	−0.198	2.526	58.3	0.865
Xylitol PB + Tz (B2)	47.52	6.119	694.59	7.9719	−0.206	2.980	52.7	0.713
Xylitol PB + Tz + MSA (B3)	47.67	5.665	880.50	6.8301	−0.221	3.054	50.6	0.670

Table 3. Electrochemical properties along with surface characteristics of electroless copper baths (a) B1, (b) B2, (c) B3, (d) B4, and (e) B5.

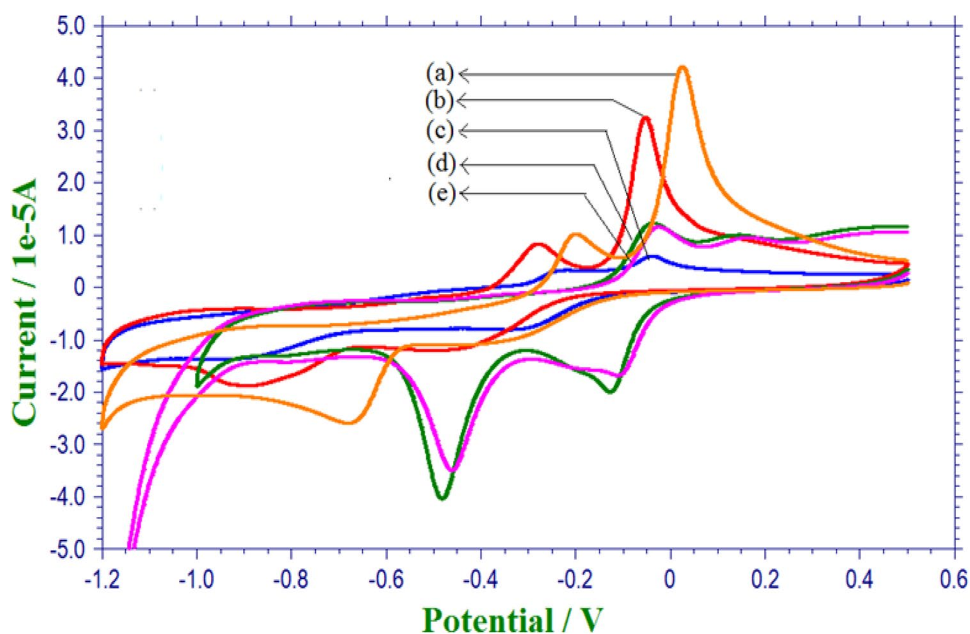

Fig. 3. Electroless copper bath cyclic voltammograms using xylitol (**a**) B1, (**b**) B2, (**c**) B3, (**d**) B4, and (**e**) B5. The Ag/AgCl (3 M KCl) electrode serves as the reference for all potentials.

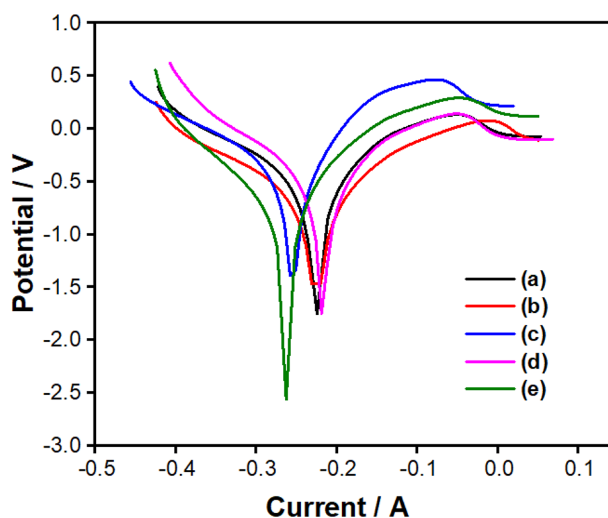

Fig. 4. Tafel polarization graphs of xylitol (**a**) B1, (**b**) B2, (**c**) B3, (**d**) B4, and (**e**) B5 electroless copper baths. The Ag/AgCl (3 M KCl) electrode serves as the reference for all potentials.

Electroless copper coatings with lower corrosion current density (icorr) values demonstrate higher corrosion resistance. An indicator of the rate of corrosion is called icorr. Table 3 shows that the results show exceptional corrosion resistance, superior plating quality, and enhanced stability under difficult circumstances.

The anodic branch, where the slope (βa) progressively decreases from PB to CS-modified baths, reflects copper dissolution and suggests improved passivation behavior. On the other hand, the cathodic branch (βc) steepens with additions, suggesting better reduction kinetics associated with altered nucleation locations and smoother surfaces. Sharper cathodic slopes and smaller anodic slopes work together to reduce active corrosion and enable more controlled copper ion reduction in the enhanced baths. The identified peaks stand for the anodic (Ipa-1) and cathodic (Ipc-1) current densities. Every curve is shown as current density (mA cm^{-2}).

Conclusion

The study effectively showed how to create five different electroless copper baths based on xylitol, each with special ingredients that affect the characteristics of the copper deposits. It was demonstrated that stabilizers and other additives functioned as efficient inhibitors by lowering physical characteristics like thickness and deposition rate. AFM surface topography testing revealed that the additions significantly reduced the roughness of the copper coatings. The roughness parameter (Ra) decreased as more chemicals were introduced; the brightener bath yielded the smoothest surface, suggesting improved adhesion, less resistance, and a higher-quality film overall. Copper films from the stabilizer and simple baths clearly favored the (111) plane, according to X-ray diffraction (XRD) studies; however, this preference shifted toward the (200) plane when MSA was added to the latter baths. This shift was attributed to changes in surface energy and an increase in copper ion concentration, which changed the crystalline structure and orientation of the copper deposits. Additionally, measurements of the crystallite size, dislocation density, and lattice parameters were performed, and the results fit the recognized criteria.

Electrochemical studies using cyclic voltammetry (CV) and Tafel polarization curves revealed that the copper coatings had remarkable corrosion resistance, exhibiting reduced corrosion current densities and improved stability under challenging conditions. The results showed that the additives enhanced the plating process and resulted in superior copper coatings with enhanced resistance to corrosion and texture. All things considered, the combination of surface investigation, electrochemical evaluation, and crystallographic analysis confirms the additives' effectiveness in enhancing the performance, stability, and quality of electroless copper films.

Data availability

The datasets used and/or analysed during the current study available from the corresponding author on reasonable request.

Received: 16 October 2025; Accepted: 7 January 2026
Published online: 23 January 2026

References

1. Varzaru, G., Savu, M., Mihailescu, B., Ionescu, C. & Branzei, M. Investigating the use of solderless assembly for electronics of some electrically conductive composite materials. *Recent Pro. Sci. Tech.* **8**, 153–175. https://doi.org/10.9734/bpi/rpst/v8/18843D (2023).
2. Giurlani, W. et al. Electroplating for decorative applications: Recent trends in research and development. *Coatings* **8**, 260. https://doi.org/10.3390/coatings8080260 (2018).
3. Zhou, Q. et al. Effect of Ni^{2+} concentration on microstructure and bonding capacity of electroless copper plating on carbon fibers. *J. Alloys Compd.* **863**, 158467. https://doi.org/10.1016/j.jallcom.2020.158467 (2021).
4. Barshilia, H. C. Surface modification technologies for aerospace and engineering applications: current trends, challenges and future prospects. *Trans Indian Natl. Acad. Eng.* **6**, 173–188. https://doi.org/10.1007/s41403-021-00208-z (2021).
5. Kostrada, A. Effectiveness of metal coating using electroplating electroless plating, and hot dipping in the manufacture of weapons. *Int. J. Soc. Serv. Res.* **3**, 1494–1498. https://doi.org/10.46799/ijssr.v3i6.399 (2023).
6. Tian, J. et al. Printable and filament-drawable PDMS-based adhesive assisted manufacturing of highly conductive copper micro-patterns. *J. Colloid Interface Sci.* **677**, 130–139. https://doi.org/10.1016/j.jcis.2024.08.068 (2025).
7. Gugua, E. C., Ujah, C. O., Asadu, C. O., Von Kallon, D. V. & Ekwueme, B. N. Electroplating in the modern era, improvements and challenges: A review. *Hybrid Adv.* **7**, 100286. https://doi.org/10.1016/j.hybadv.2024.100286 (2024).
8. Melentiev, R., Yudhanto, A., Tao, R., Vuchkov, T. & Lubineau, G. Metallization of polymers and composites: State-of-the-art approaches. *Mater. Des.* **221**, 110958. https://doi.org/10.1016/j.matdes.2022.110958 (2022).
9. Balaramesh, P., Jayalakshmi, S., Fdo, S. A., Anitha, V. & Venkatesh, P. Thin film to nano copper deposition by special additives on an eco-friendly electroless bath. *Mater. Today Proc.* **47**, 1862–1867. https://doi.org/10.1016/j.matpr.2021.03.513 (2021).
10. Kepeniene, V., Stagniunaite, R., Stalnioniene, I. & Norkus, E. Influence of temperature on electroless copper deposition from formaldehyde-containing solutions using 2-hydroxy-1,2,3-propanetricarboxylic acid as Cu (II) ligand. *ECS Trans.* **64**, 25–34. https://doi.org/10.1149/06430.0025ecst (2015).
11. Jayalakshmi, S. et al. The effect of chelators on additives in the surface characterization and electrochemical properties of an eco-friendly electroless copper nano deposition. *Sci. Rep.* **13**, 11062. https://doi.org/10.1038/s41598-023-38115-8 (2023).
12. Jiang, T. et al. Electroless copper plating on a cotton surface: Effect of metal ion ligand stability constant on reduction deposition. *Langmuir* **40**, 16283–16290. https://doi.org/10.1021/acs.langmuir.4c01455 (2024).
13. Bragaglia, M., Paleari, L., Mariani, M. & Nanni, F. Sustainable formaldehyde-free copper electroless plating on carbon-epoxy substrates. *J. Mater. Sci. Mater. Electron.* **35**, 707. https://doi.org/10.1007/s10854-024-12493-9 (2024).
14. Qin, W. & Guo, R. Metallization of polyester fabric by autocatalytic copper plating process using glyoxylic acid as a reducing agent. *Fibers Polym.* **16**, 1671–1675. https://doi.org/10.1007/s12221-015-4943-4 (2015).
15. Guo, R. Preparation of copper-coated polyester fabric via electroless plating using glyoxylic acid as reducing agent. *J. Fiber Bioeng. Inform.* **8**, 321–327. https://doi.org/10.3993/jfbim00100 (2015).
16. Balaramesh, P. et al. Influence of conventional and sustainable electroless baths on autocatalytic copper deposition. *Sci. Rep.* **15**, 33338. https://doi.org/10.1038/s41598-025-19231-z (2025).
17. Qin, W. F. Development of metallised polyester fabric by electroless copper for aircraft application using glyoxylic acid as reductant. *Trans. IMF* **94**, 246–249. https://doi.org/10.1080/00202967.2016.1163064 (2016).

18. Gwon, Y. R., Lee, J.-Y., Kim, Y. & Choe, S. Electrodeposition of compact silver from ligand-free methanesulfonic acid-based electrolyte containing copper ions. *Mater. Chem. Phys.* **326**, 129832. https://doi.org/10.1016/j.matchemphys.2024.129832 (2024).
19. Fdo, S. A., Venkatesh, P. & BalaRamesh, P. Electroless copper deposition using 3-mercaptopropionic acid as an additive. *Mater. Today Proc.* **47**, 1883–1886. https://doi.org/10.1016/j.matpr.2021.03.583 (2021).
20. Balaramesh, P., Jayalakshmi, S., Fdo, S. A., Anitha, V. & Venkatesh, P. Influence of organosulphur additives on autocatalytic copper thin film deposition. *Mater. Today Proc.* **47**, 2020–2024. https://doi.org/10.1016/j.matpr.2021.04.212 (2021).
21. Abbadi, A., Rácz, A. & Bokányi, L. Exploring the comminution process of waste printed circuit boards in recycling: A review. *J. Mater. Cycles Waste Manag.* **26**, 1326–1348. https://doi.org/10.1007/s10163-024-01945-3 (2024).
22. Hong, Y. et al. Air-plasma surface modification of epoxy resin substrate to improve electroless copper plating of printed circuit board. *Vacuum* **170**, 108967. https://doi.org/10.1016/j.vacuum.2019.108967 (2019).
23. Ghosh, S. Electroless copper deposition: A critical review. *Thin Solid Films* **669**, 641–658. https://doi.org/10.1016/j.tsf.2018.11.016 (2019).
24. Zhang, J. et al. Discovery and optimization of 1,2,4-triazole derivatives as novel ferroptosis inhibitors. *Eur. J. Med. Chem.* **284**, 117192. https://doi.org/10.1016/j.ejmech.2024.117192 (2025).
25. Pawar, K. & Dixit, P. A critical review of copper electroless deposition on glass substrates for microsystems packaging applications. *Surf. Eng.* **38**, 576–617. https://doi.org/10.1080/02670844.2022.2142002 (2022).
26. Nagireddi, S., Golder, A. K. & Uppaluri, R. Role of EDTA on the Pd(II) adsorption characteristics of chitosan cross-linked 3-amino-1,2,4-triazole-5-thiol derivative from synthetic electroless plating solutions. *Int. J. Biol. Macromol.* **127**, 320–329. https://doi.org/10.1016/j.ijbiomac.2019.01.033 (2019).
27. Cordonier, C. E. J. et al. Formation of micrometer-scale metal structures on glass by selective electroless plating on photopatterned titanium and copper-containing films. *Langmuir* **33**, 14571–14579. https://doi.org/10.1021/acs.langmuir.7b03329 (2017).
28. Ajiboye, T. O., Ajiboye, T. T., Marzouki, R. & Onwudiwe, D. C. The versatility in the applications of dithiocarbamates. *Int. J. Mol. Sci.* **23**, 1317. https://doi.org/10.3390/ijms23031317 (2022).
29. Seidi, F., Saeb, M. R., Huang, Y., Akbari, A. & Xiao, H. Thiomers of chitosan and cellulose: Effective biosorbents for detection, removal, and recovery of metal ions from aqueous medium. *Chem. Rec.* **21**, 1876–1896. https://doi.org/10.1002/tcr.202100068 (2021).
30. Pustovalov, V. K., Astafyeva, L. G. & Fritzsche, W. Optical properties of core-shell nanoparticles and their application for effective absorption, scattering, extinction, and filtering solar and optical radiation. *Phot. Nano. Fund. Appl.* **62**, 101312. https://doi.org/10.1016/j.photonics.2024.101312 (2024).
31. He, D., Qin, H., Qian, L., Sun, L. & Li, J. Conductive chitosan nonwoven fabrics by electroless plating with excellent laundering durability for wearable electronics. *J. Nat. Fibers* **19**, 14855–14865. https://doi.org/10.1080/15440478.2022.2069190 (2022).
32. Wei, C. et al. Electroless deposition of automatically shedded thin copper foils. *ACS Appl. Mater. Interfaces* **12**, 28831–28839. https://doi.org/10.1021/acsami.0c05987 (2020).
33. Langford, J. I. & Wilson, A. J. C. Scherrer after sixty years: A survey and some new results in the determination of crystallite size. *J. Appl. Crystallogr.* **11**, 102–113. https://doi.org/10.1107/s0021889878012844 (1978).
34. Williamson, G. K. & Hall, W. H. X-ray line broadening from field aluminium and wolfram. *Acta Metall.* **1**, 22–31. https://doi.org/10.1016/0001-6160(53)90006-6 (1953).
35. Ungár, T. Dislocation densities, arrangements and character from X-ray diffraction experiments. *Mater. Sci. Eng. A.* **309–310**, 14–22. https://doi.org/10.1016/S0921-5093(00)01685-3 (2001).
36. Skold, R. V. & Larson, T. E. Measurement of the instantaneous corrosion rate by means of polarization data. *Corrosion* **13**, 69–72. https://doi.org/10.5006/0010-9312-13.2.69 (1957).

Acknowledgements

This work was supported by the National Research Foundation of Korea (NRF) grant funded by the Korean government (MSIT) (RS-2025-22222973).

Author contributions

Palanivelu Balaramesh: formal analysis, writing—original draft. Raja Venkatesan: methodology, investigation, writing—original draft. Suseela Jayalakshmi: investigation, data curation. Shanmugam Kotteswaran: resources, software. Eswaran Kamaraj: conceptualization, data curation, writing—review and editing. Alexandre A. Vetcher: investigation, writing—original draft. Seong-Cheol Kim: supervision, project administration, funding acquisition, writing—review and editing. All authors have read and agreed to the published version of the manuscript.

Declarations

Competing interests

The authors declare no competing interests.

Consent to participate

All person named as author in this manuscript have participated in the planning, design and performance of the research and in the interpretation of the result.

Consent for publication

All authors have indorsed the publication of this research.

Additional information

Correspondence and requests for materials should be addressed to P.B., R.V. or S.-C.K.

Reprints and permissions information is available at www.nature.com/reprints.

Publisher's note Springer Nature remains neutral with regard to jurisdictional claims in published maps and institutional affiliations.

Open Access This article is licensed under a Creative Commons Attribution-NonCommercial-NoDerivatives 4.0 International License, which permits any non-commercial use, sharing, distribution and reproduction in any medium or format, as long as you give appropriate credit to the original author(s) and the source, provide a link to the Creative Commons licence, and indicate if you modified the licensed material. You do not have permission under this licence to share adapted material derived from this article or parts of it. The images or other third party material in this article are included in the article's Creative Commons licence, unless indicated otherwise in a credit line to the material. If material is not included in the article's Creative Commons licence and your intended use is not permitted by statutory regulation or exceeds the permitted use, you will need to obtain permission directly from the copyright holder. To view a copy of this licence, visit http://creativecommons.org/licenses/by-nc-nd/4.0/.

© The Author(s) 2026